

Dynamic Metasurface Antennas for MIMO-OFDM Receivers with Bit-Limited ADCs

Hanqing Wang, Nir Shlezinger, Yonina C. Eldar, Shi Jin,
Mohammadreza F. Imani, Insang Yoo, and David R. Smith

Abstract

The combination of orthogonal frequency modulation (OFDM) and multiple-input multiple-output (MIMO) systems plays an important role in modern communication systems. In order to meet the growing throughput demands, future MIMO-OFDM receivers are expected to utilize a massive number of antennas, operate in dynamic environments, and explore high frequency bands, while satisfying strict constraints in terms of cost, power, and size. An emerging technology to realize massive MIMO receivers of reduced cost and power consumption is based on dynamic metasurface antennas (DMAs), which inherently implement controllable compression in acquisition. In this work we study the application of DMAs for MIMO-OFDM receivers operating with bit-constrained analog-to-digital converters (ADCs). We present a model for DMAs which accounts for the configurable frequency selective profile of its metamaterial elements, resulting in a spectrally flexible hybrid structure. We then exploit previous results in task-based quantization to show how DMAs can be configured to improve recovery in the presence of constrained ADCs, and propose methods for adjusting the DMA parameters based on channel state information. Our numerical results demonstrate that the DMA-based receiver is capable of accurately recovering OFDM signals. In particular, we show that by properly exploiting the spectral diversity of DMAs, notable performance gains are obtained over existing designs of conventional hybrid architectures, demonstrating the potential of DMAs for MIMO-OFDM setups in realizing high performance massive antenna arrays of reduced cost and power consumption.

Index terms— Metasurface antennas, quantization, MIMO-OFDM.

This project has received funding from the Benozio Endowment Fund for the Advancement of Science, the Estate of Olga Klein – Astrachan, the European Unions Horizon 2020 research and innovation program under grant No. 646804-ERC-COG-BNYQ, and the Air Force Office of Scientific Research under grants No. FA9550-18-1-0187 and FA9550-18-1-0208. H. Wang and S. Jin are with the National Mobile Communications Research Lab, Southeast University, Nanjing, P. R. China (e-mail: {hqwanglyt; jinshi}@seu.edu.cn). N. Shlezinger and Y. C. Eldar are with the Faculty of Math and CS, Weizmann Institute of Science, Rehovot, Israel (e-mail: {nir.shlezinger; yonina}@weizmann.ac.il). M. F. Imani, I. Yoo, and D. R. Smith are with the Department of ECE, Duke University, Durham, NC (e-mail: mohamad.imani@gmail.com; {insang.yoo, drsmith}@duke.edu).

I. INTRODUCTION

Wireless networks are subject to constantly growing throughput demands. To satisfy these requirements, cellular base stations (BSs) are equipped with a large number of antennas while serving multiple remote users [1], utilizing wideband orthogonal frequency division multiplexing (OFDM) transmissions. Such multi-user (MU) multiple-input multiple-output (MIMO) OFDM architectures are capable of reliably providing increased data rates to a large amount of users [2].

In addition to their performance requirements, BSs are expected to be cost efficient, operate under strict power constraints, and support deployment in various physical shapes and sizes. A major challenge associated with realizing such MU-MIMO-OFDM systems stems from the increased cost of analog-to-digital convertors (ADCs) [3], which allow the analog signals observed by each antenna to be processed in digital. The power usage of an ADC is related to the signal bandwidth and the number of bits used for digital representation [4]. Thus, when the number of antennas and ADCs operating at wide bands is large, limiting the number of bits, thus operating under quantization constraints, is crucial to keep feasible cost and power usage [5].

Focusing on uplink communications, quantization constraints imply that the BS cannot process the channel output directly but rather a discretized distorted representation of it. The distortion induced by the continuous-to-discrete quantization mapping degrades the ability to extract the desired information, such as recovering the transmitted signal, from the observed channel output. An attractive strategy to mitigate the effect of quantization error is to incorporate pre-quantization processing in analog resulting in a hybrid architecture. Jointly designing the analog processing along with the quantization rule and the digital mapping, referred to as *task-based quantization*, was shown to facilitate recovery of the underlying information in the digital domain [6]–[8]. An advantage of such hybrid MIMO receivers, originally proposed as a method to decrease the number of radio frequency (RF) chains [9]–[12], is that they can be used to reduce the number of quantized samples, and accordingly, the number of ADCs, compared to assigning an ADC to each antenna [13]. Nonetheless, such designs require an additional dedicated hardware [14], and the pre-quantization mapping, as well as the ability to adapt its parameters based on the channel conditions, is typically limited and dictated by the analog components [10], [11].

An alternative receiver architecture which implements adjustable analog combining in the hardware level is based on dynamic metasurface antennas (DMAs) [15], [16]. Such surfaces consist of a set of microstrips, each embedded with configurable radiating metamaterial elements

[17], [18]. Recent years have witnessed a growing interest in the application of metasurfaces as reflecting surfaces for wireless communications [19]–[23]. In such applications, a metasurface is placed in a physical location where it can aid the BS by reflecting and steering the transmitted waveforms. Metasurfaces utilized as antennas in wireless communications, i.e., as transmitting and receiving devices rather than configurable reflectors, were recently studied in [24]–[26]. Such antenna structures typically use much less power and cost less than architectures based on standard arrays [27], while facilitating the implementation of a large number of tunable elements in a given physical area [28]. In the context of wireless communications, it is shown in [24], [25] that the achievable rate when utilizing DMAs without quantization constraints is comparable to using ideal antenna arrays. The potential of DMAs for realizing massive MIMO antennas combined with the need of such systems to operate with low resolution quantization motivates the study of bit-constrained DMA-based BSs, which is the focus of the current work.

Here, we study uplink MU-MIMO-OFDM communications in which a bit-constrained BS is equipped with a DMA. We first extend the model formulated in [24], which was built upon approximations of the DMA properties proposed in [15] that hold for narrowband signals, to faithfully capture the reconfigurable frequency selective nature of DMAs in wideband setups, such as OFDM systems. Then, we show how the resulting DMA characteristics can be incorporated into the MU-MIMO-OFDM model, resulting in a form of a hybrid receiver. However, while conventional hybrid architectures require a dedicated analog combining hardware whose mapping is typically frequency flat [9]–[11], [14], [29]–[32], DMAs implement a controllable frequency selective profile as an inherent byproduct of their antenna structure. We use this model to formulate the following problem: How can the dynamic properties of DMAs, i.e., their configurable reception parameters, be exploited to facilitate the task of recovering the transmitted OFDM signals from the output of low-resolution ADCs?

Based on this formulation, we cast the problem as a task-based quantization setup, in which the task is to accurately recover the transmitted OFDM symbols. Using this framework, we derive a scheme for jointly optimizing the DMA weights along with the quantization system, i.e., the ADC support and the digital processing, under a given bit constraint. Our proposed method consists of three algorithms. The first algorithm utilizes a greedy optimization method to tune the DMA weights, ignoring the structure constraints induced by the physics of these metasurfaces. The next two algorithms then identify a feasible approximation of the unconstrained DMA obtained using the first algorithm, where each technique applies to a different DMA model: The first of

these two methods is based on the approximations of DMA characteristics proposed in [15], which ignore the spectral flexibility of the elements, tuning a frequency flat hybrid receiver most suitable for narrowband signals; The latter makes usage of the full frequency selective profile of the metamaterial elements, and is thus preferable for wideband transmissions. Both proposed algorithms exploit the unique structure of the hybrid system which arises from the task-based quantization framework, while building upon the dynamic nature of DMAs, which allows to set their parameters in run-time in light of the channel conditions.

The performance of the resulting receivers designed using these proposed algorithms, in terms of OFDM signal recovery accuracy and uncoded bit error rate (BER), are evaluated in a simulation study. Our numerical results demonstrate the ability of bit-constrained DMAs to achieve notable performance gains over conventional hybrid architectures designed using previously proposed methods. These performance gains, which arise from the combination of task-based quantization tools and the spectral flexibility of DMAs, add to their practical benefits over conventional hybrid structures, which follow from the fact that DMAs do not require additional dedicated hardware for implementing their analog processing.

The rest of this paper is organized as follows: Section II presents the system model of DMA-based receivers in bit-constrained MIMO-OFDM systems, introducing the formulation of the configurable frequency selectivity of the metamaterial elements and how it is incorporated in the wireless communication setup. Section III details the proposed DMA design methods along with a discussion. Numerical examples are presented in Section IV. Finally, Section V concludes the paper. Proofs of the results stated in the paper are detailed in the appendix.

Throughout the paper, we use boldface lower-case letters for vectors, e.g., \mathbf{x} ; Matrices are denoted with boldface upper-case letters, e.g., \mathbf{M} ; and calligraphic letters are used for sets, where \mathcal{C} and \mathcal{Z} are the complex numbers and integers, respectively. The ℓ_2 norm, Kronecker product, transpose, Hermitian transpose, conjugate, and trace are denoted by $\|\cdot\|$, \otimes , $(\cdot)^T$, $(\cdot)^H$, $(\cdot)^*$, and $\text{tr}[\cdot]$, respectively. We use \mathbf{I}_n and \mathbf{O}_n for the $n \times n$ identity matrix and all-zero matrix, respectively. Finally, $\text{blkdiag}(\mathbf{A}_1, \dots, \mathbf{A}_n)$ is a block diagonal matrix with the matrices $\mathbf{A}_1, \dots, \mathbf{A}_n$ along its diagonal.

II. SYSTEM MODEL

In this section, we present the mathematical model for DMA-based uplink MU-MIMO-OFDM systems with bit-constrained ADCs. We begin with the model for the DMA operation in

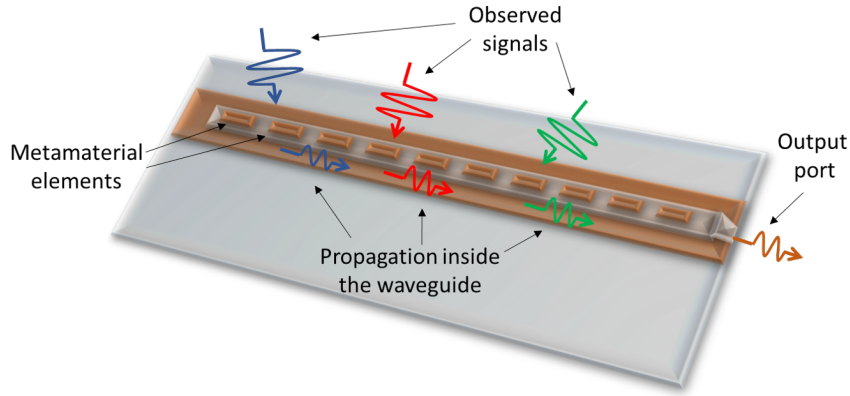


Fig. 1. Illustration of signal reception using a microstrip.

Subection II-A, which extends the one proposed in our previous work [24] to fully capture the frequency selective characteristics of metasurfaces used as antennas. Then, in Subsection II-B, we formulate the input-output relationship of coarsely quantized uplink MU-MIMO-OFDM systems in which the BS is equipped with a DMA.

A. *Dynamic Metasurface Antennas*

Metamaterials are a class of artificial materials whose physical properties, such as their permittivity and permeability, can be externally configured to achieve some desired electromagnetic properties [33]. Metamaterial elements stacked in surface configurations are referred to as metasurfaces. These two-dimensional structures can be tuned element-wise, allowing the metasurface to carry out desired operations, such as radiation, reflection, beamforming, and reception of propagating waves [34]. In particular, metasurfaces can be utilized as antennas by incorporating such surfaces on top of a guiding structure. A simple and common metasurface antenna architecture is comprised of a set of microstrips, each consisting of a multitude of sub-wavelength, frequency-dependent resonant metamaterial radiating elements [35], whose radiation properties are dynamically adjustable. A larger antenna array can be thus formed by increasing the number of microstrips, or alternatively, by tiling several such metasurface antennas together.

When used as a receive antenna, the signals observed by the elements are captured at a single output port for each microstrip, feeding an RF chain and an ADC with Nyquist rate sampling. An illustration of a set of observed signals captured using a single microstrip is depicted in Fig. 1. The relationship between these signals and the microstrip output is dictated by the following two properties:

P1 Each element acts as resonant electrical circuit, whose frequency response is described by the Lorentzian form [15], [16]:

$$\alpha(f) = \frac{F \cdot f^2}{(f^R)^2 - f^2 - j\chi f}, \quad (1)$$

where $F > 0$ is the oscillator strength, $f^R > 0$ is the resonance frequency, and $\chi > 0$ is the damping factor. In DMAs, these parameters can be varied by external control for each element individually [17].

P2 Since the output port is located on the edge of the microstrip while the elements are uniformly placed along it, each signal which propagates from an element to that port undergoes a different path, and thus accumulates a different delay, depending on the specific element. In particular, letting β be the wavenumber along the microstrip and ρ_l denote the location of the l th element, this phase shift can be modeled as a filter whose frequency response is proportional to $e^{-j\beta\rho_l}$.

To facilitate the configuration of DMAs, the frequency response of the metamaterial elements in *P1* is often assumed to be *frequency flat*, i.e., $\alpha(f) \equiv \alpha$ for each considered f , commonly representing narrowband signals. Under this assumption, the ability to externally control the response of the elements is typically modeled as allowing to set any $\alpha \in [a_{\min}, a_{\max}]$ for some $0 < a_{\min} < a_{\max}$, referred to as *amplitude-only weights* [15, Sec. III-A], or alternatively, $\alpha \in \{\frac{j+e^{j\phi}}{2} | \phi \in [0, 2\pi]\}$, referred to as *Lorentzian-constrained phase weights* [15, Sec. III-D]. Our previous work [24] used this frequency invariance assumption to analyze the achievable rate of uplink DMA-based MIMO systems. Here, as we consider wideband OFDM signals, we adopt the general model in (1) rather than its simplified narrowband approximation. In particular, by controlling the resonance frequency f^R and the damping factor χ , one can obtain a variety of different frequency selective profiles for each element.

As an example, we depict in Figs. 2-3 the frequency response of a single element with magnitude normalized to unity at resonance, i.e., $\frac{\alpha(f)}{\alpha(f^R)}$, in which the ratio $\frac{f^R}{\chi}$, referred to as the quality factor, is fixed to 50. The frequency response is evaluated for several different resonance frequencies f^R , focusing on the frequency band around 1.9 GHz. Observing Figs. 2-3, we note that each element approximates a bandpass filter, by setting its resonance frequency to be within the observed bandwidth, or alternatively, a filter with a frequency monotonic and even a frequency flat profile, when f^R is outside of the band of interest. In the sequel we show that this frequency

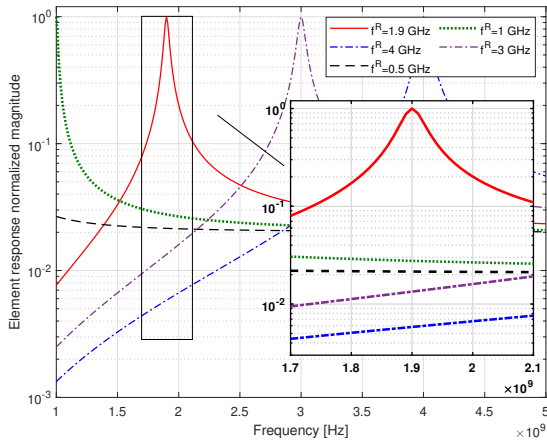


Fig. 2. Element response magnitude vs. frequency.

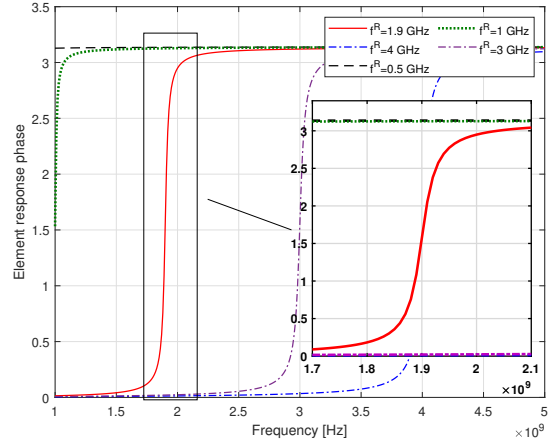


Fig. 3. Element response phase vs. frequency.

selectivity can be exploited to facilitate OFDM signal recovery in the presence of quantized measurements.

Processing of the DMA output is carried out in digital baseband. Therefore, we next formulate the resulting model in discrete-time. Consider a DMA with $N \triangleq N_d \cdot N_e$ tunable metamaterial elements, where N_d and N_e are the number of microstrips and elements in each microstrip, respectively. Let $y_{i,l}[t]$ denote the equivalent baseband signal received from the wireless channel on metamaterial element l of microstrip i at time slot $t \in \{0, 1, \dots, M-1\} \triangleq \mathcal{M}$, where M is the transmission block size, and let $y_{i,l}(\omega)$ be its discrete-time Fourier transform (DTFT). The frequency domain representation of the output of the i th microstrip, denoted $z_i(\omega)$ can be written as

$$z_i(\omega) = \sum_{l=1}^{N_e} h_{i,l}(\omega) q_{i,l}(\omega) y_{i,l}(\omega), \quad (2)$$

where $h_{i,l}(\omega)$ characterizes the effect of the signal propagation inside the microstrip $P2$, while $q_{i,l}(\omega)$ denotes the tunable weight of the l th element of the i th microstrip. Based on property PI , this frequency dependent profile, which represents the DTFT equivalent of (1), is given by

$$q_{i,l}(\omega) = \frac{F_{i,l} \Omega^2(\omega)}{(\Omega_{i,l}^R)^2 - \Omega^2(\omega) - j\Omega(\omega)\chi_{i,l}}. \quad (3)$$

In the above equation, $F_{i,l}$, $\chi_{i,l}$, and $\Omega_{i,l}^R$ are the configurable oscillator strength, damping factor, and angular resonance frequency, respectively, of the l th element of microstrip i . We use $\Omega(\omega)$ to denote the analogous angular frequency corresponding to the continuous-time frequency ω , namely, how the bandwidth of interest in continuous-time is mapped into angular frequencies of the DTFT of the discrete-time signal. This mapping is dictated by the carrier frequency f_c and

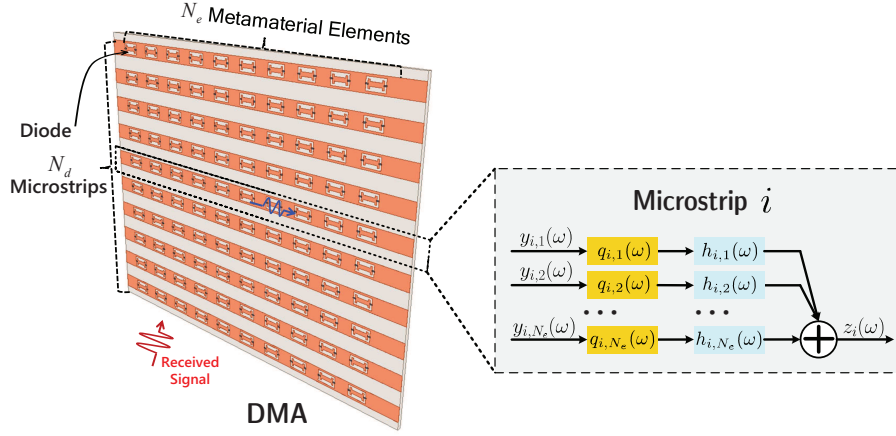


Fig. 4. DMA model illustration.

the sampling rate f_s , and can be written as

$$\Omega(\omega) = 2\pi f_c + \omega f_s, \quad |\omega| < \pi.$$

An illustration of the system is given in Fig. 4.

Next, we express the DMA model in (2) compactly in vector form. To that aim, we define a set of $N \times N$ diagonal matrices $\mathbf{H}(\omega)$ whose $[(i-1)N_e + l]$ th diagonal element is $h_{i,l}(\omega)$. We also define $\mathbf{y}(\omega) \in \mathcal{C}^N$ as the vector comprised of the frequency domain received signal of the complete array such that its $[(i-1)N_e + l]$ th element is $y_{i,l}(\omega)$. Using these definitions and letting $\mathbf{z}(\omega) \in \mathcal{C}^{N_d}$ be the DTFT of the DMA output, i.e., $(\mathbf{z}(\omega))_i = z_i(\omega)$, the frequency domain formulation of the DMA operation can be formulated as

$$\mathbf{z}(\omega) = \mathbf{Q}(\omega)\mathbf{H}(\omega)\mathbf{y}(\omega), \quad (4)$$

where the matrix $\mathbf{Q}(\omega) \in \mathcal{C}^{N_d \times N}$ represents the tunable weights, and its entries are given by $(\mathbf{Q}(\omega))_{k,(i-1)N_e+l} = q_{i,l}(\omega)$ when $i = k$, and 0 when $i \neq k$, where $l \in \{1, 2, \dots, N_e\} \triangleq \mathcal{N}_e$ and $i, k \in \{1, 2, \dots, N_d\} \triangleq \mathcal{N}_d$. By its definition, $\mathbf{Q}(\omega)$ is block diagonal with diagonal blocks being row vectors denoted by $(\mathbf{q}_i(\omega))^T = [q_{i,1}(\omega), q_{i,2}(\omega), \dots, q_{i,N_e}(\omega)] \in \mathcal{C}^{N_e}$ for $i \in \mathcal{N}_d$. The vector expression (4) is utilized to formulate bit-constrained DMA-based MU-MIMO-OFDM systems, as detailed in the next subsection.

B. Received Signal Model

In this paper, we consider the uplink scenario of a single-cell MU-MIMO-OFDM system. Here, the BS is equipped with a DMA consisting of N_d microstrips with a total of $N =$

$N_e \cdot N_d$ metamaterial elements, and serves K single-antenna users. The users simultaneously transmit OFDM symbols with M subcarriers each. Due to power or memory constraints, the BS processes a coarsely quantized version of the DMA output obtained using ADCs, modeled as identical uniform scalar quantizers with resolution b . In particular, we focus on the recovery of the transmitted OFDM symbols in a hybrid manner by jointly configuring the DMA weights along with a digital filter applied to the ADCs outputs.

We consider a frequency-selective wireless channel, which follows a tapped delay line model with L_G taps, represented by a set of $K \times N$ matrices $\{\mathbf{G}[\tau]\}_{\tau=0}^{L_G-1}$. Let $\mathbf{s}[t] \in \mathcal{C}^K$ be the OFDM symbols transmitted at the t th time slot, assumed to be i.i.d. and with covariance matrix \mathbf{I}_K . We focus on time instances $t \in \mathcal{M}$, which correspond to the OFDM block after cyclic prefix (CP) removal. We denote the DTFT of $\{\mathbf{G}[\tau]\}_{\tau=0}^{L_G-1}$ and $\{\mathbf{s}[t]\}_{t=0}^{M-1}$ as $\mathbf{G}(\omega)$ and $\mathbf{s}(\omega)$, respectively. Then, the DTFT representation of the received channel output vector $\mathbf{y}(\omega)$ is expressed as

$$\mathbf{y}(\omega) = \mathbf{G}(\omega)\mathbf{s}(\omega) + \mathbf{w}(\omega), \quad (5)$$

where $\mathbf{w}(\omega) \in \mathcal{C}^N$ is the DTFT of the additive noise vectors $\{\mathbf{w}[t]\}_{t=0}^{M-1}$, which are independent of $\mathbf{s}[t]$ and follow a zero-mean proper-complex Gaussian distribution with covariance \mathbf{C}_W for each ω . Since the elements in every microstrip are commonly sub-wavelength spaced, they are typically spatially correlated, and thus \mathbf{C}_W is not restricted to be diagonal. The combined effect of the wireless channel and the propagation inside the microstrips in the frequency domain can be represented by the equivalent channel $\hat{\mathbf{G}}(\omega) = \mathbf{H}(\omega)\mathbf{G}(\omega)$.

We assume the CP length is larger than the memory length of the equivalent channel $\hat{\mathbf{G}}(\omega)$. Consequently, the frequency response of all considered signals and channels is fully captured by its M -point discrete Fourier transform (DFT), i.e., the DTFT in angular frequencies $\{\omega_m \triangleq \frac{2\pi m}{M}\}_{m \in \mathcal{M}}$. For brevity, we henceforth write $\hat{\mathbf{G}}_m \triangleq \hat{\mathbf{G}}_m(\omega_m)$, and similarly define \mathbf{Q}_m , \mathbf{H}_m , \mathbf{z}_m , \mathbf{s}_m and \mathbf{w}_m . Using the above notations and substituting (4) into (5) for all M subchannels, the input-output relationship of a single OFDM block after CP removal in the frequency domain can be written in matrix form in which each row represents a single frequency bin via

$$\bar{\mathbf{Z}} = \bar{\mathbf{Q}}\bar{\mathbf{G}}\bar{\mathbf{S}} + \bar{\mathbf{Q}}\bar{\mathbf{H}}\bar{\mathbf{W}}, \quad (6)$$

where $\bar{\mathbf{Z}} \triangleq [\mathbf{z}_0^T, \mathbf{z}_1^T, \dots, \mathbf{z}_{M-1}^T]^T$, $\bar{\mathbf{S}} \triangleq [\mathbf{s}_0^T, \mathbf{s}_1^T, \dots, \mathbf{s}_{M-1}^T]^T$, and $\bar{\mathbf{W}} \triangleq [\mathbf{w}_0^T, \mathbf{w}_1^T, \dots, \mathbf{w}_{M-1}^T]^T$ denote the vertically concatenated vectors of the DMA output, transmitted signal and additive

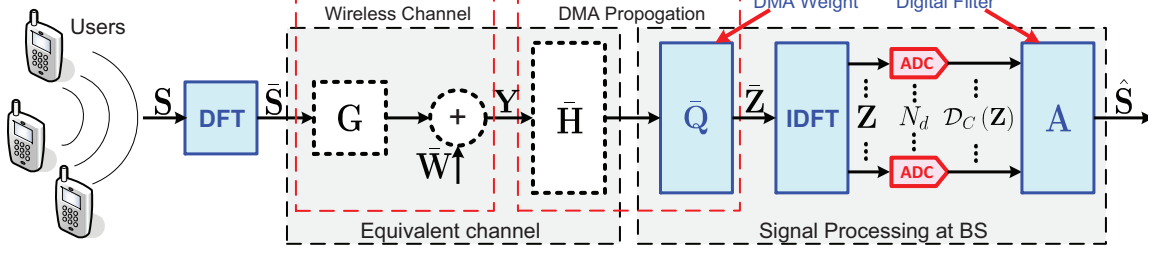


Fig. 5. Illustration of signal processing procedure. The configurable receiver parameters are the digital filter \mathbf{A} , the DMA weights $\bar{\mathbf{Q}}$, and the ADC support γ .

noise observed on each subchannel, respectively; $\bar{\mathbf{Q}} \triangleq \text{blkdiag}(\mathbf{Q}_0, \mathbf{Q}_1, \dots, \mathbf{Q}_{M-1})$, $\bar{\mathbf{G}} \triangleq \text{blkdiag}(\hat{\mathbf{G}}_0, \hat{\mathbf{G}}_1, \dots, \hat{\mathbf{G}}_{M-1})$ and $\bar{\mathbf{H}} \triangleq \text{blkdiag}(\mathbf{H}_0, \mathbf{H}_1, \dots, \mathbf{H}_{M-1})$ denote the block diagonal formulation of DMA weights, equivalent channel and DMA propagation characterization on each subchannel, respectively. The expression (6) models the DMA output, which is fed to the ADCs, in the frequency domain. Since the ADC operation is formulated in the time domain, we transform $\bar{\mathbf{Z}}$ into the time domain by multiplying it with $\mathbf{V}_1 \triangleq (\mathbf{F}_M^H \otimes \mathbf{I}_{N_d})$, where \mathbf{F}_M is the $M \times M$ normalized DFT matrix. The resulting DMA output is given by:

$$\mathbf{Z} = (\mathbf{F}_M^H \otimes \mathbf{I}_{N_d}) \bar{\mathbf{Z}} = \mathbf{V}_1 \bar{\mathbf{Q}} \bar{\mathbf{G}} \mathbf{V}_2 \mathbf{S} + \mathbf{V}_1 \bar{\mathbf{Q}} \bar{\mathbf{H}} \bar{\mathbf{W}}, \quad (7)$$

where in (7) we used the definitions $\mathbf{V}_2 \triangleq (\mathbf{F}_M \otimes \mathbf{I}_K)$, $\mathbf{S} = [\mathbf{s}[0]^T, \mathbf{s}[1]^T, \dots, \mathbf{s}[M-1]^T]^T$, and $\mathbf{Z} = [\mathbf{z}[0]^T, \mathbf{z}[1]^T, \dots, \mathbf{z}[M-1]^T]^T$.

The DMA outputs $\{\mathbf{z}[t]\}_{t=0}^{M-1}$ are quantized using N_d identical pairs of ADCs which independently discretize the real and imaginary parts of each analog input sample. We denote the complex-valued quantization mapping by $\mathcal{D}_C(x+jy) = \mathcal{D}(x) + j\mathcal{D}(y)$, where $\mathcal{D}(\cdot)$ is the uniform real-valued quantization operator with support γ , i.e.,

$$\mathcal{D}(x) = \begin{cases} -\gamma + \frac{2\gamma}{b} \left(l + \frac{1}{2} \right) & x - l \cdot \frac{2\gamma}{b} + \gamma \in \left[0, \frac{2\gamma}{b} \right], l \in \{0, 1, \dots, b-1\}, \\ \text{sign}(x) \left(\gamma - \frac{\gamma}{b} \right) & |x| > \gamma. \end{cases} \quad (8)$$

The recovered symbols are obtained by linearly processing the quantized DMA outputs. Letting the \mathbf{A} represent the digital linear processing, the resulting estimate of \mathbf{S} is expressed by

$$\hat{\mathbf{S}} = \mathbf{A} \mathcal{D}_C(\mathbf{Z}). \quad (9)$$

An illustration of the overall system is depicted in Fig. 5. It is noted that resulting formulation models the processing of the received signal as a bit-constrained hybrid system with frequency

selective analog combining, represented by the weights $\bar{\mathbf{Q}}$. As such, the system in Fig. 5 specializes a broad range of conventional hybrid receiver architectures, in which the analog processing is frequency flat, e.g., [9]–[11]. For example, this model specializes bit-constrained hybrid receivers with partially-connected phase shifter networks, as considered in [29], by fixing $\mathbf{H}(\omega)$ to be the identity matrix, i.e., canceling the effect of the propagation inside the microstrips $P2$, while restricting the elements $q_{i,l}(\omega)$ of which $\bar{\mathbf{Q}}$ is comprised to be independent of ω and have a unit magnitude, namely, $q_{i,l}(\omega) \equiv e^{j\phi_{i,l}}$ for some $\phi_{i,l} \in [0, 2\pi)$ for all $(i, l) \in \mathcal{N}_d \times \mathcal{N}_e$.

Our aim is to jointly design the DMA weights $\bar{\mathbf{Q}}$, the digital linear filter \mathbf{A} , and the ADC support γ to minimize the symbol recovery mean-squared error (MSE) $\mathbb{E}\{\|\mathbf{S} - \hat{\mathbf{S}}\|^2\}$, namely to produce an accurate estimate of \mathbf{S} . The estimator $\hat{\mathbf{S}}$ can be then used to facilitate the detection of each symbol, taking values in some discrete constellation.

III. DMA DESIGN

We now propose a DMA configuration scheme to minimize the signal recovery MSE. Our method is derived by treating the joint design of the DMA weights and the digital filter as a task-based quantization setup [6]. We first formulate the problem accordingly in Subsection III-A. Then, in Subsection III-B we propose a greedy method for configuring the DMA weights assuming that they can take any frequency selective profile. Next, we show in Subsection III-C how these unconstrained weights can be used to choose a DMA with approximately frequency flat weights, as assumed in [24], as well as elements obeying the more general Lorentzian frequency selective profile, as stated in property *P1*. Finally, we discuss some of the insights and related aspects which arise from these designs in Subsection III-D.

A. Task-Based Quantization Formulation

Task-based quantization refers to the joint optimization of the quantization rule along with its pre and post quantization mappings in light of a given system task [6]–[8], [13]. The bit-constrained receiver architecture detailed in Subsection II-B can be treated as a task-based quantization setup, since the output of the wireless channel is acquired and discretized for the task of recovering the transmitted OFDM symbols. In particular, the formulations of the DMA output in (7) and the estimated symbols in (9) indicate that the DMA induces a configurable pre-quantization mapping, represented by the matrix $\mathbf{V}_1\bar{\mathbf{Q}}$, while the filter \mathbf{A} corresponds to the digital post-quantization processing. Using this framework, we next characterize the achievable

OFDM recovery accuracy for a given DMA configuration, which is used in the following subsection to derive algorithms for setting the DMA weights.

Following [6], we derive $\bar{\mathbf{Q}}$ and \mathbf{A} assuming that the ADCs are not overloaded, i.e., that the magnitudes of the real and imaginary parts of \mathbf{Z} are not larger than the ADC support γ , with sufficiently large probability. To guarantee this, we set γ to be some multiple $\eta > 0$ of the maximal standard deviation of the ADC inputs, such that the overload probability is bounded via Chebyshev's inequality [36, Pg. 64]. This setting can be expressed as

$$\begin{aligned} \gamma^2 &= \eta^2 \max_{t \in \mathcal{M}} \max_{i \in \mathcal{N}_d} \mathbb{E}\{ |(\mathbf{z}[t])_i|^2 \} \\ &\stackrel{(a)}{=} \eta^2 \max_{i \in \mathcal{N}_d} \frac{1}{M} \sum_{t \in \mathcal{M}} \mathbb{E}\{ |(\mathbf{z}[t])_i|^2 \} \stackrel{(b)}{=} \eta^2 \max_{i \in \mathcal{N}_d} \frac{1}{M} \sum_{m \in \mathcal{M}} \mathbb{E}\{ |(\mathbf{z}_m)_i|^2 \} \\ &= \eta^2 \max_{i \in \mathcal{N}_d} \frac{1}{M} \sum_{m \in \mathcal{M}} \mathbf{q}_{m,i}^T \mathbf{E}_i^T \mathbf{\Upsilon}_m \mathbf{E}_i \mathbf{q}_{m,i}^*, \end{aligned} \quad (10)$$

where (a) follows from the stationarity of baseband OFDM symbols after CP removal [37], and (b) is obtained from Parseval's equality. In (10), \mathbf{E}_i represents the selection of the microstrip, and is given by $\mathbf{E}_i = [\mathbf{E}_{i,1}, \mathbf{E}_{i,2}, \dots, \mathbf{E}_{i,N_d}]^T$ with $\mathbf{E}_{i,i} = \mathbf{I}_{N_e}$ while $\mathbf{E}_{i,j} = \mathbf{O}_{N_e}$ for $j \neq i$. The matrix $\mathbf{\Upsilon}_m$ is the covariance of the equivalent channel output at frequency bin $m \in \mathcal{M}$, given by $\mathbf{\Upsilon}_m \triangleq \hat{\mathbf{G}}_m \hat{\mathbf{G}}_m^H + \mathbf{H}_m \mathbf{C}_W \mathbf{H}_m^H$. The MSE-minimizing digital filter for a fixed $\bar{\mathbf{Q}}$ with non-overloaded ADCs, and its corresponding MSE for asymptotically large M are stated in the following lemma:

Lemma 1. *The MSE minimizing digital filter \mathbf{A} under a fixed DMA configuration $\bar{\mathbf{Q}}$ and ADC support γ is given by*

$$\mathbf{A}^*(\bar{\mathbf{Q}}) = \mathbf{V}_2^H \bar{\mathbf{G}}^H \bar{\mathbf{Q}}^H (\sigma_q^2 \mathbf{I}_{MN_d} + \bar{\mathbf{Q}} \mathbf{\Sigma} \bar{\mathbf{Q}}^H)^{-1} \mathbf{V}_1^H, \quad (11)$$

where $\sigma_q^2 \triangleq \frac{4\gamma^2}{3b^2}$ represents the quantization noise energy, and $\mathbf{\Sigma} \triangleq \text{blkdiag}(\mathbf{\Upsilon}_0, \mathbf{\Upsilon}_1, \dots, \mathbf{\Upsilon}_{M-1})$. The corresponding MSE is $\text{EMSE}(\bar{\mathbf{Q}}) + e^\circ$, where e° is the minimal MSE (MMSE) in recovering \mathbf{S} from the channel output, and the excess MSE is

$$\text{EMSE}(\bar{\mathbf{Q}}) = \text{tr} \left[\bar{\mathbf{G}}^H \mathbf{\Sigma}^{-1} (\mathbf{\Sigma}^{-1} + \sigma_q^{-2} \bar{\mathbf{Q}}^H \bar{\mathbf{Q}})^{-1} \mathbf{\Sigma}^{-1} \bar{\mathbf{G}} \right]. \quad (12)$$

Proof: The asymptotic Gaussianity of OFDM signals [38] implies that the MMSE estimate of \mathbf{S} is linear when the number of subcarriers M is asymptotically large. Consequently, in that

regime, the linear estimator of \mathbf{S} from the channel output achieves the MMSE e° , and thus the problem of identifying $\mathbf{A}^*(\bar{\mathbf{Q}})$ and its corresponding MSE is a special case of [6, Lemma 1], formulated for complex-valued signals. ■

It follows from the proof of Lemma 1 that the requirement of M to be asymptotically large is necessary to guarantee that the MMSE estimate of \mathbf{S} from the channel output is linear, namely, that the transmitted OFDM symbols approach being Gaussian. Consequently, the lemma also rigorously holds for finite M when the entries of \mathbf{S} obey a jointly Gaussian distribution, i.e., the transmitters utilize Gaussian symbols, as commonly assumed in the massive MIMO literature [1], [39], [40].

Lemma 1 characterizes the achievable MSE of the DMA-based BS in recovering the OFDM signals matrix \mathbf{S} for a given DMA weights $\bar{\mathbf{Q}}$. While the excess MSE in (12) holds rigorously for non-overloaded ADCs and asymptotically large number of subcarriers, it also constitutes a close approximation of the error for systems with a finite number of subcarriers and a small but not necessarily zero probability of overloading the quantizers under a broad range of channel output distributions [6], and is thus used in the following as an objective function for setting the DMA weights. Nonetheless, determining the feasible DMA configuration which minimizes the excess MSE in (12) is a challenging task. Particularly, the constraints on the structure of $\bar{\mathbf{Q}}$ and the feasible values of its entries, as well as the expression of the objective function (12), make the derivation of a tractable closed-form expression for the MSE-minimizing DMA weights difficult. However, the problem can be simplified by accounting for the block diagonal structure of $\{\mathbf{Q}_m\}_{m=0}^{M-1}$ and Σ . Specifically, \mathbf{Q}_m^H is a block diagonal matrix of column vectors $\{\mathbf{q}_{m,i}^*\}_{i=1}^{N_d}$, namely, $\mathbf{Q}_m^H = \text{blkdiag}(\mathbf{q}_{m,1}^*, \mathbf{q}_{m,2}^*, \dots, \mathbf{q}_{m,N_d}^*)$. As a result, $\mathbf{Q}_m^H \mathbf{Q}_m$ is also a block diagonal matrix comprised of the rank-one submatrices $\{\mathbf{q}_{m,i}^* \mathbf{q}_{m,i}^T\}_{i=1}^{N_d}$ along its main diagonal. This structure leads to the following formulation of the excess MSE:

Proposition 1. *The excess MSE (12) can be written as*

$$\text{EMSE}(\bar{\mathbf{Q}}) = \sum_{m=1}^M \text{tr} \left[\hat{\mathbf{G}}_m^H \Upsilon_m^{-1} \left(\Upsilon_m^{-1} + \sigma_q^{-2} \sum_{i=1}^{N_d} \mathbf{E}_i \mathbf{q}_{m,i}^* \mathbf{q}_{m,i}^T \mathbf{E}_i^T \right)^{-1} \Upsilon_m^{-H} \hat{\mathbf{G}}_m \right]. \quad (13)$$

Proof: See Appendix A.

The alternative formulation of $\text{EMSE}(\bar{\mathbf{Q}})$ allows to optimize the vectors $\{\mathbf{q}_{m,i}\}$ individually in a greedy manner, instead of the matrix $\bar{\mathbf{Q}}$ directly. Based on this strategy, we next propose a DMA configuration algorithm.

B. Greedy Unconstrained DMA Configuration

We next propose a DMA weight design strategy based on the objective (13). We note that recovering the weights which minimize (13) is difficult due to the constrained feasible set, modeled via property *PI*, and the fact that the excess MSE (13) is not separable in the microstrip index $i \in \mathcal{N}_d$. Therefore, our design approach consists of two steps: First, we propose a greedy method for optimizing the weights individually for each sub-channel $m \in \mathcal{M}$, assuming unconstrained weights, i.e., that the frequency response can be set for each element at each frequency bin individually. Then, we show how these unconstrained weights can be approximated using a feasible DMA configuration in the following subsection.

When the DMA weights can be tuned individually in each frequency bin, the problem of configuring the elements is formulated as

$$\{\mathbf{q}_{m,i}\}_{i=1}^{N_d} = \arg \min_{\{\bar{\mathbf{q}}_i \in \mathcal{C}^{N_e}\}} \text{tr} \left[\hat{\mathbf{G}}_m^H \mathbf{\Upsilon}_m^{-1} \left(\mathbf{\Upsilon}_m^{-1} + \sigma_q^{-2} \sum_{i'=1}^{N_d} \mathbf{E}_{i'} \bar{\mathbf{q}}_{i'}^* \bar{\mathbf{q}}_{i'}^T \mathbf{E}_{i'}^T \right)^{-1} \mathbf{\Upsilon}_m^{-H} \hat{\mathbf{G}}_m \right]. \quad (14)$$

Due to the difficulty in optimizing (14) jointly for the weights of all the microstrips, i.e., over all $i \in \mathcal{N}_d$, we set the weights associated with each microstrip separately, updating the complete DMA in a sequential manner. In particular, the method operates iteratively, where in the i th iteration, we account for the contribution of the i th microstrip to the MSE and optimize its weight vector $\mathbf{q}_{m,i}$ given the previously designed weights $\{\mathbf{q}_{m,j}\}_{j=1}^{i-1}$. To formulate the greedy method, define $\mathbf{U}_{m,0} \triangleq \mathbf{\Upsilon}_m^{-1}$ and $\mathbf{U}_{m,i} \triangleq \mathbf{\Upsilon}_m^{-1} + \sigma_q^{-2} \sum_{j=1}^i \mathbf{E}_j \mathbf{q}_{m,j}^* \mathbf{q}_{m,j}^T \mathbf{E}_j^T$ for $i \geq 1$, which can be written as $\mathbf{U}_{m,i} = \mathbf{U}_{m,i-1} + \sigma_q^{-2} \mathbf{E}_i \mathbf{q}_{m,i}^* \mathbf{q}_{m,i}^T \mathbf{E}_i^T$. The MSE in (14) can now be computed by recursively evaluating

$$\begin{aligned} J_{m,i} &= \text{tr} \left[\hat{\mathbf{G}}_m^H \mathbf{\Upsilon}_m^{-1} \left(\mathbf{U}_{m,i-1} + \sigma_q^{-2} \mathbf{E}_i \mathbf{q}_{m,i}^* \mathbf{q}_{m,i}^T \mathbf{E}_i^T \right)^{-1} \mathbf{\Upsilon}_m^{-1} \hat{\mathbf{G}}_m \right] \\ &\stackrel{(a)}{=} \text{tr} \left[\hat{\mathbf{G}}_m^H \mathbf{\Upsilon}_m^{-1} \mathbf{U}_{m,i-1}^{-1} \mathbf{\Upsilon}_m^{-1} \hat{\mathbf{G}}_m \right] - \frac{\mathbf{q}_{m,i}^T \mathbf{\Xi}_{m,i} \mathbf{q}_{m,i}^*}{\sigma_q^2 + \mathbf{q}_{m,i}^T \mathbf{\Psi}_{m,i} \mathbf{q}_{m,i}^*}, \end{aligned} \quad (15)$$

where (a) follows from the Sherman-Morisson formula [41, Ch. 3.8], and we define $\mathbf{\Xi}_{m,i} \triangleq \mathbf{E}_i^T \mathbf{U}_{m,i-1}^{-1} \mathbf{\Upsilon}_m^{-1} \hat{\mathbf{G}}_m \hat{\mathbf{G}}_m^H \mathbf{\Upsilon}_m^{-1} \mathbf{U}_{m,i-1}^{-1} \mathbf{E}_i$ and $\mathbf{\Psi}_{m,i} \triangleq \mathbf{E}_i^T \mathbf{U}_{m,i-1}^{-1} \mathbf{E}_i$. Note that $J_{m,i}$ in (15) coincides with the objective in (14) for $i = N_d$. Our proposed greedy approach sequentially selects $\mathbf{q}_{m,i}$ that minimizes $J_{m,i}$, which is equivalent to maximizing the second term of (15), given that $\{\mathbf{q}_{m,j}\}_{j=1}^{i-1}$ have been determined in the previous iterations, i.e., that $\mathbf{U}_{m,i-1}$ is known. Note that the quantization noise energy σ_q^2 , which depends on the ADC support γ , is determined by

the complete matrix $\bar{\mathbf{Q}}$ via (10). To facilitate the minimization of $J_{m,i}$ with respect to $\mathbf{q}_{m,i}$ for every $i \in \mathcal{N}_d$, we optimize each $\mathbf{q}_{m,i}$ assuming that γ in σ_q^2 is dictated by the output of the i th microstrip at the m th frequency bin, i.e., $\gamma^2 = \eta^2 \mathbb{E}\{|\mathbf{z}_m)_i|^2\}$. By defining $\kappa \triangleq \frac{4\eta^2}{3b^2}$ and substituting (10) into (15), the resulting optimization problem becomes

$$\mathbf{q}_{m,i} = \arg \max_{\mathbf{q} \in \mathcal{C}^{N_e}} \bar{J}_{m,i}(\mathbf{q}) \triangleq \frac{\mathbf{q}^T \Xi_{m,i} \mathbf{q}^*}{\mathbf{q}^T (\kappa \mathbf{E}_i^T \Upsilon_m \mathbf{E}_i + \Psi_{m,i}) \mathbf{q}^*}. \quad (16)$$

The solution of (16) is characterized in the following lemma:

Lemma 2. *The solution to (16) is given by $\alpha_{m,i} \hat{\mathbf{q}}_{m,i}$ for any $\alpha_{m,i} \in \mathcal{C}$, where $\hat{\mathbf{q}}_{m,i}^*$ is the generalized eigenvector corresponding to the maximal generalized eigenvalue of $\Xi_{m,i}$ and $\kappa \mathbf{E}_i^T \Upsilon_m \mathbf{E}_i + \Psi_{m,i}$.*

Proof: This lemma follows from [42, Sec 4.5]. ■

Lemma 2 indicates that when $\kappa \mathbf{E}_i^T \Upsilon_m \mathbf{E}_i + \Psi_{m,i}$ is invertible, then $\hat{\mathbf{q}}_{m,i}$ is the conjugate of the eigenvector corresponding to the largest eigenvalue of $(\kappa \mathbf{E}_i^T \Upsilon_m \mathbf{E}_i + \Psi_{m,i})^{-1} \Xi_{m,i}$. The resulting greedy algorithm is summarized as Algorithm 1. The fact that the solution in Lemma 2 is invariant to the value of $\alpha_{m,i}$ is exploited to facilitate its projection into a feasible DMA weight vector, as detailed next.

Algorithm 1: Greedy unconstrained DMA configuration

Input: Channel parameters Υ_m and $\hat{\mathbf{G}}_m$ for $m \in \mathcal{M}$;
ADC parameter κ .

Init: $\mathbf{U}_{m,0} = \Upsilon_m^{-1}$ for each $m \in \mathcal{M}$.

```

1 for  $i = 1, 2, \dots, N_d$  do
2   for  $m = 1, 2, \dots, M$  do
3     Set  $\hat{\mathbf{q}}_{m,i}$  from  $\mathbf{U}_{m,i-1}$  using Lemma 2;
4     Set  $\mathbf{U}_{m,i} = \mathbf{U}_{m,i-1} + (\kappa \hat{\mathbf{q}}_{m,i}^T \mathbf{E}_i^T \Upsilon_m \mathbf{E}_i \hat{\mathbf{q}}_{m,i})^{-1} \mathbf{E}_i \hat{\mathbf{q}}_{m,i}^* \hat{\mathbf{q}}_{m,i}^T \mathbf{E}_i^T$ ;
5   end
6 end

```

Output: Unconstrained weights $\{\hat{\mathbf{q}}_{m,i}\}, (m, i) \in \mathcal{M} \times \mathcal{N}_d$.

C. Setting Feasible DMA Weights

Here, we approximate the unconstrained configuration computed via Algorithm 1, denoted $\{\hat{\mathbf{q}}_{m,i}\}$, using a feasible DMA setting, i.e., one whose elements satisfy the model detailed in Subsection II-A. In particular, we wish to set the DMA weights to minimize the distance of each element response from its corresponding unconstrained value, exploiting the invariance

of each microstrip weights to a scalar factor, noted in Lemma 2. Following the frequency selective element model (3), and defining $\Omega_m \triangleq \Omega(\omega_m)$, the resulting optimization problem can be expressed as the following non-linear least squares formulation:

$$\{\hat{F}_{i,l}, \hat{\chi}_{i,l}, \hat{\Omega}_{i,l}^R\} = \arg \min_{\{F_{i,l}, \chi_{i,l}, \Omega_{i,l}^R\}} \min_{\{\alpha_{m,i}\}} \sum_{i=1}^{N_d} \sum_{l=1}^{N_e} \sum_{m=1}^M \left| \frac{F_{i,l} \Omega_m^2}{(\Omega_{i,l}^R)^2 - \Omega_m^2 - j\Omega_m \chi_{i,l}} - \alpha_{m,i} (\hat{\mathbf{q}}_{m,i})_l \right|^2. \quad (17)$$

Directly solving (17) is a challenging task due to its non-convex structure and the fact that the objective is not separable in the frequency index $m \in \mathcal{M}$. Therefore, in the following we first seek a feasible approximation assuming that the weights are fixed to be frequency flat, as in [24]. Then, we show how the method can be extended to properly tune the frequency selective profile of each element as in (17).

1) *Frequency-Flat Weights*: Frequency flat weights is an approximation for the element frequency response which holds under narrowband signals, or alternatively, when the resonance frequency is far from the band of interest. In such cases, elements exhibit the same frequency response which takes values in some set \mathcal{Q} , for all considered frequency bins, e.g., $\mathcal{Q} = [a_{\min}, a_{\max}]$ for amplitude-only weights. Under this approximation, we denote the weights of each microstrip of index $i \in \mathcal{N}_d$ by a column vector $\mathbf{q}_i \in \mathcal{Q}^{N_e}$, which is designed to approximate the unconstrained solutions $\{\hat{\mathbf{q}}_{m,i}\}$ for each microstrip separately by solving

$$\mathbf{q}_i = \arg \min_{\mathbf{q} \in \mathcal{Q}^{N_e}} \min_{\{\alpha_{m,i}\}_{m=1}^M} \sum_{m=1}^M \|\mathbf{q} - \alpha_{m,i} \hat{\mathbf{q}}_{m,i}\|^2, \quad i \in \mathcal{N}_d. \quad (18)$$

We tackle the optimization problem (18) in an alternating manner based on the following lemma:

Lemma 3. *For a fixed $\mathbf{q}_i \in \mathcal{C}^{N_e}$, (18) is minimized by setting $\alpha_{m,i} = \frac{\mathbf{q}_i^T \hat{\mathbf{q}}_{m,i}^*}{\|\hat{\mathbf{q}}_{m,i}\|^2}$ for all $m \in \mathcal{M}$. Additionally, for fixed $\{\alpha_{m,i}\}$, (18) can be solved element-wise for each $l \in \mathcal{N}_e$ via*

$$(\mathbf{q}_i)_l = \arg \min_{q \in \mathcal{Q}} \sum_{m=1}^M |q - \alpha_{m,i} (\hat{\mathbf{q}}_{m,i})_l|^2. \quad (19)$$

Proof: The Lemma is obtained by repeating the arguments used in [24, Appendix B]. ■

For $\mathcal{Q} = \mathcal{C}$, the value $q \in \mathcal{Q}$ which minimizes (19) is given by $\hat{q}_{i,l} = \frac{1}{M} \sum_{m=1}^M \alpha_{m,i} (\hat{\mathbf{q}}_{m,i})_l$. In our algorithm we thus set the entries $(\mathbf{q}_i)_l$ by projecting $\hat{q}_{i,l}$ into the feasible set \mathcal{Q} . Lemma 3 and (19) imply that the non-uniqueness of $\alpha_{m,i}$ can be utilized to obtain frequency-invariant feasible approximations of the frequency-selective unconstrained weights $\hat{\mathbf{q}}_{m,i}$ via alternating optimization. In particular, for each microstrip index $i \in \mathcal{N}_d$, the unconstrained weights are

projected into a feasible set, and the resulting approximation is used to compute the weights of the remaining microstrips via the greedy method. The detailed procedure of the proposed DMA configuration scheme is summarized in Algorithm 2. Once the DMA weights matrix $\bar{\mathbf{Q}}$ is assigned, it is used to determine the ADC support γ and the digital filter via (10) and (11), respectively.

Algorithm 2: Frequency-flat setting

Input: Unconstrained weights $\{\hat{\mathbf{q}}_{m,i}\}$, $m \in \mathcal{M}$, $i \in \mathcal{N}_d$;
alternating iterations limit iter_{\max} .

Init: $\alpha_{m,i} = 1$ for all $(m,i) \in \mathcal{M} \times \mathcal{N}_d$.

1 **for** $i = 1, 2, \dots, N_d$ **do**

2 **for** $\text{iter} = 1, 2, \dots, \text{iter}_{\max}$ **do**

3 Set the elements of \mathbf{q}_i by projecting $\frac{1}{M} \sum_{m=1}^M \alpha_{m,i} (\hat{\mathbf{q}}_{m,i})_l$ into \mathcal{Q} ;

4 Set $\{\alpha_{m,i}\}_{m=1}^M$ using Lemma 3;

5 **end**

6 **end**

Output: $\mathbf{Q}_m = \text{blkdiag}(\mathbf{q}_1^T, \mathbf{q}_2^T, \dots, \mathbf{q}_{N_d}^T)$ for all $m \in \mathcal{M}$.

2) *Frequency-Selective Weights:* While recovering a frequency flat DMA configuration via Algorithm 2 is relatively simple, it does not exploit the ability of the DMA elements to tune a frequency selective profile in light of the system objective. However, directly solving the non-convex optimization problem (17) to recover the parameters $\{F_{i,l}, \chi_{i,l}, \Omega_{i,l}^R\}$ of each element is a difficult task. Therefore, as in the frequency flat case, we again adopt an alternating optimization approach. However, here we also account for our understanding of what types of frequency selective profiles are realized using such metamaterial elements.

In particular, we note that the parameters $\{\alpha_{m,i}\}$ which minimize the objective (17) for fixed $\{F_{i,l}, \chi_{i,l}, \Omega_{i,l}^R\}$ are obtained using Lemma 2. Similarly, for fixed $\{\chi_{i,l}, \Omega_{i,l}^R\}$ and $\{\alpha_{m,i}\}$, the oscillation strength values of the elements can be tuned based on the following lemma:

Lemma 4. *For fixed $\{\chi_{i,l}, \Omega_{i,l}^R\}$ and $\{\alpha_{m,i}\}$, the non-negative element oscillation strength values which minimize the right hand side of (17) are given by*

$$\hat{F}_{i,l} = \text{Re} \left(\sum_{m=1}^M \frac{\Omega_m^2 \alpha_{m,i}^* (\hat{\mathbf{q}}_{m,i})_l^*}{(\Omega_{i,l}^R)^2 - \Omega_m^2 - j\Omega_m \chi_{i,l}} \right)^+ \cdot \left(\sum_{m=1}^M \frac{\Omega_m^4}{((\Omega_{i,l}^R)^2 - \Omega_m^2)^2 + \Omega_m^2 \chi_{i,l}^2} \right)^{-1}, \quad (20)$$

where $(x)^+ \triangleq \max(x, 0)$.

Proof: The lemma follows from [24, Lemma 2]. ■

We are now left with identifying a method for setting the parameters $\{\chi_{i,l}, \Omega_{i,l}^R\}$, which essentially control how the response of each element varies in frequency. The non-convexity of (17) in those parameters implies classical non-linear least squares curve fitting methods, e.g., the LevenbergMarquardt algorithm [43] or gradient descent, are likely to yield a local minima, unless properly initialized. In order to select an initial point for curve fitting, let us recall that, as shown in Subsection II-A and demonstrated in Figs. 2-3, the Lorentzian function describing the frequency response of the l th element of microstrip i (3) represents one of the following three families of frequency selective profiles:

- 1) *Monotonically decreasing magnitude* - achieved by setting the resonance frequency $\Omega_{i,l}^R$ to be smaller than the lowest frequency in the band of interest. In particular, setting $\Omega_{i,l}^R = 0$ and $\chi_{i,l} = 0$ yields amplitude-only frequency flat weights.
- 2) *Monotonically increasing magnitude* - such profiles are obtained by setting $\Omega_{i,l}^R$ to be larger than the maximal frequency in the band of interest, where the slope is determined by how far $\Omega_{i,l}^R$ is from the band of interest.
- 3) *Unimodal profile* - when $\Omega_{i,l}^R$ is within the considered frequency band, the element resembles a unimodal function, i.e., a bandpass filter, centered at $\Omega_{i,l}^R$.

In addition to the aforementioned profiles, which describe the spectral behavior of the magnitude of the elements frequency response, it is also noted that the phase of (3) is always in the upper half of the complex plain, i.e., in the range $[0, \pi]$, as also observed in Fig. 3.

The feasible spectral profiles indicate which types of unconstrained weights are best captured by DMA elements. In particular, if for some $(i, l) \in \mathcal{N}_d \times \mathcal{N}_e$, the unconstrained weights $\{\alpha_{m,i}(\hat{\mathbf{q}}_{m,i})_l\}_{n \in \mathcal{M}}$ exhibit a decreasing magnitude, then it is likely they can be well-approximated by the output of non-linear least squares solver starting from a resonance frequency smaller than the lower edge of the band of interest, e.g., $\Omega_{i,l}^R = f_c - f_s/2 - \Delta$, for some fixed $\Delta > 0$. Similarly, when the behavior of $\{\alpha_{m,i}(\hat{\mathbf{q}}_{m,i})_l\}_{n \in \mathcal{M}}$ resembles a monotonic increase in magnitude, they should be accurately approached when curve fitting starting from $\Omega_{i,l}^R = f_c + f_s/2 + \Delta$. Finally, if the amplitudes of $\{\alpha_{m,i}(\hat{\mathbf{q}}_{m,i})_l\}_{n \in \mathcal{M}}$ are a unimodal curve whose peak, located in index $\tilde{m} \in \mathcal{M}$, lies in the upper half of the complex plain, then using $\Omega_{i,l}^R = \Omega_{\tilde{m}}$ as a starting point is expected to yield a close approximation of the unconstrained weights. This understanding of the spectral behavior of DMA elements can be used by choosing those three suggested initial points for gradient search optimization, and taking the setting which achieves the minimal objective

(17). This approach is summarized as Algorithm 3. As in the frequency flat case, the resulting weights $\bar{\mathbf{Q}}$ are used to determine the ADC support γ and the digital filter via (10) and (11), respectively.

Algorithm 3: Frequency-selective setting

Input: Unconstrained weights $\{\hat{\mathbf{q}}_{m,i}\}$, $m \in \mathcal{M}$, $i \in \mathcal{N}_d$;
alternating iterations limit iter_{\max} .

Init: $\alpha_{m,i} = 1$ for all $(m,i) \in \mathcal{M} \times \mathcal{N}_d$.

$F_{i,l} = 1$ for all $(i,l) \in \mathcal{N}_d \times \mathcal{N}_e$.

1 **for** $i = 1, 2, \dots, N_d$ **do**

2 **for** $\text{iter} = 1, 2, \dots, \text{iter}_{\max}$ **do**

3 **for** $l = 1, 2, \dots, N_e$ **do**

4 Set $(\Omega_{i,l}^{R,(1)}, \chi_{i,l}^{(1)})$ using a non-linear least-squares solver to fit (17) starting from
 $\Omega_{i,l}^R = f_c - f_s/2 - \Delta$;

5 Set $(\Omega_{i,l}^{R,(2)}, \chi_{i,l}^{(2)})$ using a non-linear least-squares solver to fit (17) starting from
 $\Omega_{i,l}^R = f_c + f_s/2 + \Delta$;

6 Set $(\Omega_{i,l}^{R,(3)}, \chi_{i,l}^{(3)})$ using a non-linear least-squares solver to fit (17) starting from
 $\Omega_{i,l}^R = \Omega_{\tilde{m}}$;

7 Set $(\hat{\Omega}_{i,l}^R, \hat{\chi}_{i,l})$ as the pair from $\{\Omega_{i,l}^{R,(k)}, \chi_{i,l}^{(k)}\}$ which minimizes (17);

8 Set $\hat{F}_{i,l}$ using Lemma 4;

9 **end**

10 Set $\{\alpha_{m,i}\}_{m=1}^M$ using Lemma 3;

11 **end**

12 **end**

Output: $(\mathbf{Q}_m)_{i,l} = q_{i,l}(\omega_m)$ via (3) for all $(m,i,l) \in \mathcal{M} \times \mathcal{N}_d \times \mathcal{N}_e$.

D. Discussion

DMA-based receivers, as follows from our model in Subsection II-A, implement a type of hybrid beamforming. In particular, the received signal undergoes some processing which reduces its dimensionality prior to being converted into a digital representation. Such hybrid architectures are commonly used in the massive MIMO literature, often as method to reduce the number of RF chains [10]–[12] but also to facilitate recovery under bit constraints [13]. Conventional hybrid receivers utilize an additional dedicated hardware to implement the analog combining, typically consisting of phase shifter networks, i.e., an interconnection of phase shifters and adders. One of the benefits of using DMAs over conventional hybrid architectures, also noted in [24], is that the controllable analog combining in DMAs is a natural byproduct of the antenna structure, and does not require additional dedicated hardware. Another advantage stems from the fact

that conventional hybrid systems, such as phase shifter networks, are typically frequency flat, namely, the same analog mapping is implemented for all the spectral components of the input signal [12]. The inherent adjustable frequency selectivity of the DMA elements implies that they can be tuned to apply a frequency varying analog combining, which corresponds to one of the three profiles discussed in the previous subsection. This property is expected to improve the achievable performance in wideband frequency selective setups, as numerically demonstrated in Section IV.

Furthermore, the proposed design methods are based on task-based quantization schemes, exploiting the block diagonal structure of $\bar{\mathbf{Q}}$ to yield a set of optimization problems which can be solved in a greedy fashion. This structure of $\bar{\mathbf{Q}}$ stems from the DMA architecture, which consists of several microstrips each feeding a different ADC. As the DMA operation is modeled as a form of analog beamforming, the proposed approach can also be utilized for conventional hybrid structures in which the analog combiner obeys a block diagonal model, i.e., partially connected networks [10], [29]. In these conventional architectures, the filter $\mathbf{H}(\omega)$, modeling the propagation inside the microstrips, is replaced with the identity mapping. Consequently, our approach, which is based on formulating the signal recovery problem as a task-based quantization system, is expected to also facilitate the design of standard hybrid receivers. As we focus here on DMA-based receivers, we leave the analysis of the application of our methods for tuning conventional hybrid systems for future work.

The spectral profile of the DMA elements is exploited in Algorithm 3 to achieve various types of frequency selective analog combining. In particular, the Lorentzian form (3) allows to set each element to approach a controllable bandpass filter or an approximately spectrally-linear gain. While these profiles accommodate a broad family of spectral shapes, more complex functions, such as multi-modal frequency responses, may not be closely approximated by DMAs. Furthermore, in Algorithm 3 we allowed to set the resonance frequencies $\{\Omega_{i,l}^R\}$ and the damping factors $\{\chi_{i,l}\}$ to be any non-negative values. However, setting the elements to have a large quality factor $\frac{\Omega_{i,l}^R}{\chi_{i,l}}$ may be difficult in practice, and this ratio is commonly restricted to be in the order of several tens [35]. These additional considerations can also be accounted for in the optimization of the frequency response parameters of the elements. For example, in our numerical study in Section IV we restrict the quality factor to a set of feasible values.

The algorithms detailed in the previous subsections provide methods for configuring the DMA weights along with the ADCs and the digital processing to accurately recover OFDM signals,

facilitating their decoding by the BS. This procedure requires the receiver to know the multipath channel $\mathbf{G}[\tau]$, the noise covariance \mathbf{C}_W , and the DMA frequency selectivity profile $\mathbf{H}(\omega)$. While the latter can be obtained from the physics of the metasurface, the channel parameters must be estimated, which may be a challenging task in the presence of quantized channel outputs [13], [30], [44]. When channel estimation is carried out in a time division duplexing manner, the dynamic nature of DMAs can be exploited to assign different configurations during channel estimation and signal recovery. However, we leave this study for future investigation.

IV. NUMERICAL EVALUATIONS

In this section, we numerically evaluate the performance of bit-constrained MIMO-OFDM systems in which the BS is equipped with a DMA configured using the method detailed in Section III, demonstrating the performance gains achieved by exploiting the frequency selectivity of DMAs and by treating the receiver operation as a task-based quantization setup. We consider a single-cell uplink MU-MIMO setup in which a BS serves $K = 8$ users. The users simultaneously transmit OFDM signals with central frequency $f_c = 1.9$ GHz, each comprised of $M = 16$ subcarriers with carrier spacing of 20 MHz. The data symbols are independently drawn from a QPSK constellation.

The wireless channel is generated based on the correlated Gaussian model for rich scattering environments [45] with $L_G = 4$ taps. The resulting discrete-time channel is given by $\mathbf{G}[\tau] = \sigma_{\mathbf{G}}^2[\tau] \Sigma_R^{\frac{1}{2}} \mathbf{G}_R[\tau]$, where $\{\sigma_{\mathbf{G}}^2[\tau]\}$ represents a temporal exponentially decaying profile, i.e., $\sigma_{\mathbf{G}}^2[\tau] = e^{-\tau}$; $\{\mathbf{G}_R[\tau]\}$ are $N \times K$ Rayleigh fading matrices; and Σ_R is the correlation matrix of the antenna array, induced by sub-wavelength element spacing. In particular, we set $\Sigma_R = \mathbf{I}_{N_d} \otimes \Sigma_C$, modelling the case where the microstrips are sufficiently spaced such that elements of different microstrips are not correlated, where $\Sigma_C \in \mathcal{C}^{N_e \times N_e}$ represents the spatial correlation among the elements of the same microstrip with 0.2 wavelength spacing. Following Jakes' model [46], we use $(\Sigma_C)_{i,l} = J_0(0.4\pi|i-l|)$, where $J_0(\cdot)$ is the zero-order Bessel function of the first type and $i, l \in \mathcal{N}_e$. Due to the coupling between elements, the noise is spatially correlated, and we choose $\mathbf{C}_W = \sigma_z^2 \Sigma_R$, with $\sigma_z^2 > 0$.

We consider a DMA comprised of a total $N = 100$ elements, divided into $N_d = 10$ microstrips with $N_e = 10$ elements in each. The propagation inside the microstrip, modeled via the diagonal matrix $\mathbf{H}(\omega)$, is set to $(\mathbf{H}(\omega))_{i,l} = e^{-\alpha l - j\beta(\omega)l}$, where $\alpha = 0.006$ [m⁻¹] and $\beta(\omega) = 1.592 \cdot \omega$ [m⁻¹]. This setting represents microstrips with 50 ohm characteristic impedance made of Duroid 5880

operating at 1.9 GHz with element spacing of 0.2 wavelength (assuming free space wavelength) [47, Ch. 3.8].

In the following we numerically evaluate the performance in terms of signal recovery MSE and uncoded BER of the following receivers:

- R1* A DMA with unconstrained weights designed using Algorithm 1.
- R2* A DMA whose elements obey the Lorentzian model (1), designed to approximate the unconstrained DMA setting *R1* using Algorithm 3. To guarantee that the elements are configured with a feasible quality factor, we fix the ratio $\frac{\Omega_{i,l}^R}{\chi_{i,l}}$ to be in the discrete set $[0.1, 5, 30]$, and carry out the non-linear least-squared curve fitting in Algorithm 3, implemented using the Levenberg-Marquardt method [43], with respect to the resonance frequency $\Omega_{i,l}^R$ for each $(i, l) \in \mathcal{N}_d \times \mathcal{N}_e$.
- R3* A DMA whose elements are restricted to be frequency flat, following the approximation used in [24]. In particular, we consider amplitude only weights, for which the response is selected in the range $[0.001, 1]$ to approximate the unconstrained DMA *R1* using Algorithm 2.
- R4* A hybrid receiver with a partially-connected phase shifter network designed using the method of [29], operating with fixed ADCs of support $\gamma = 100$. The support value was selected based on a set of numerical tests where it was shown to guarantee ADC overloading probability of roughly 1%. This receiver represents previously proposed hybrid architectures for bit-constrained scenarios which are not derived using the task-based quantization framework, as we do in our work.
- R5* The linear MMSE estimator for recovering the symbols from the channel output *without quantization constraints*. This receiver represents a lower bound on the achievable performance of the bit-constrained receivers *R1-R4*.

For the bit-constrained BSs *R1-R4*, we consider an overall budget of up to b_{overall} bits, divided equally among the ADCs such that each ADC operates with a resolution of $b = \lfloor 2^{b_{\text{overall}}/(2 \cdot N_d)} \rfloor$ decision regions. For the task-based quantizers *R1-R3* we used $\eta = 2$. The output of the ADCs is processed using the digital filter of Lemma 1. The results are computed by averaging over 10^3 MIMO-OFDM symbols.

We begin by evaluating the signal recovery MSE of the considered receiver structures versus the signal-to-noise ratio (SNR) in the range of $[-4, 16]$ dB, for an overall bit budget of $b_{\text{overall}} = 80$ bits. The results are depicted in Fig. 6. Observing Fig. 6, we first note that the unconstrained DMA *R1*, designed based on the task-based quantization framework of [6],

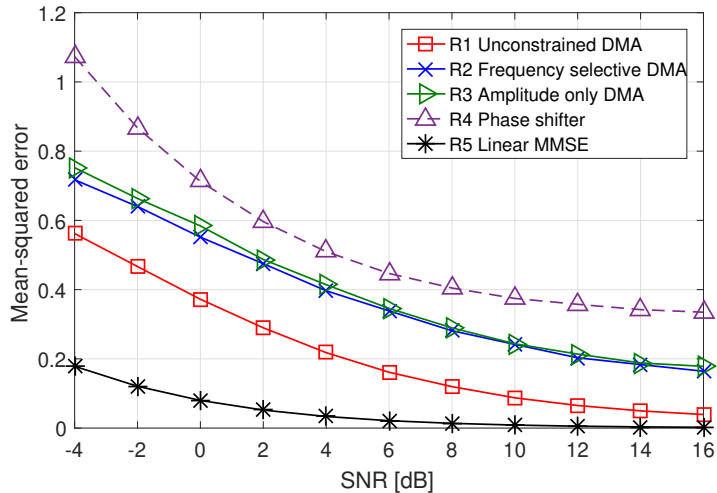


Fig. 6. MSE versus SNR, 80 overall bits.

achieves the most accurate recovery among the bit-constrained receivers, indicating that the proposed greedy method in Algorithm 1 yields useful configurations. The frequency selective DMA $R2$ designed using Algorithm 3 outperforms the frequency flat hybrid receivers $R3$ - $R4$, with substantial gains over the previously proposed phase shifter network of [29], and more minor gains over the amplitude-only DMA designed using our proposed Algorithm 2. In particular, $R2$ achieves an MSE of 0.4 at SNR of 4 dB, while the previously proposed $R4$ requires SNR of at least 8 dB to achieve the same MSE, i.e., an SNR gain of 4 dB. The corresponding SNR gain of the frequency selective $R2$ over the frequency flat $R3$, designed using our Algorithm 2, is 0.5 dB. In addition to performance gains of the DMA-based BSs over the phase shifter receiver $R4$, the latter requires additional dedicated hardware for combining the observed signals, while DMAs implements this analog combining as a natural byproduct of their antenna architecture. These results demonstrate the benefits of exploiting the physical characteristics of DMAs using a task-based quantization framework, in which the analog combining is jointly optimized with the ADC support and the digital processing.

To evaluate how the MSE improvement of our proposed approach is translated into gains in BER, we depict in Fig. 7 the uncoded BER of the above receivers versus SNR for $b_{\text{overall}} = 80$ bits. The results in Fig. 7 demonstrate that the gains in MSE observed in Fig. 6 are translated in uncoded BER improvement of a lesser magnitude. In particular, $R2$ achieves an uncoded BER of $8 \cdot 10^{-2}$ at SNR of 6 dB, while $R3$ and $R4$ achieve the same BER value for SNRs of roughly 6.5 dB and 14 dB, respectively, namely, an SNR gain of 0.5 dB and 7.5 dB, respectively.

Finally, we evaluate how the performance of the proposed DMAs configurations scales with

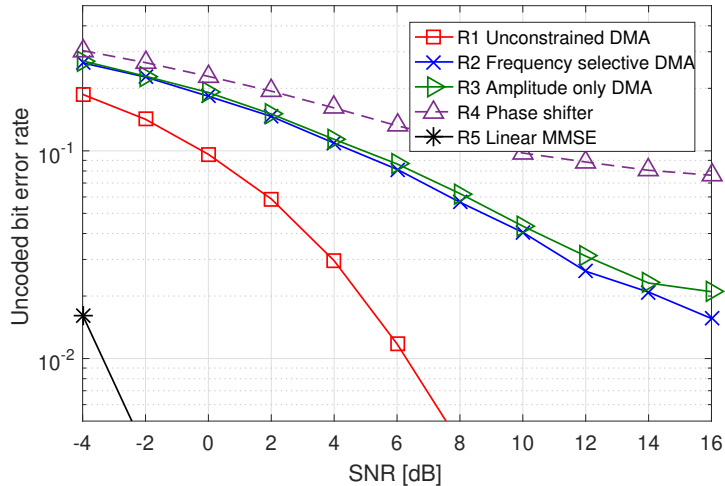


Fig. 7. Uncoded BER versus SNR, 80 overall bits.

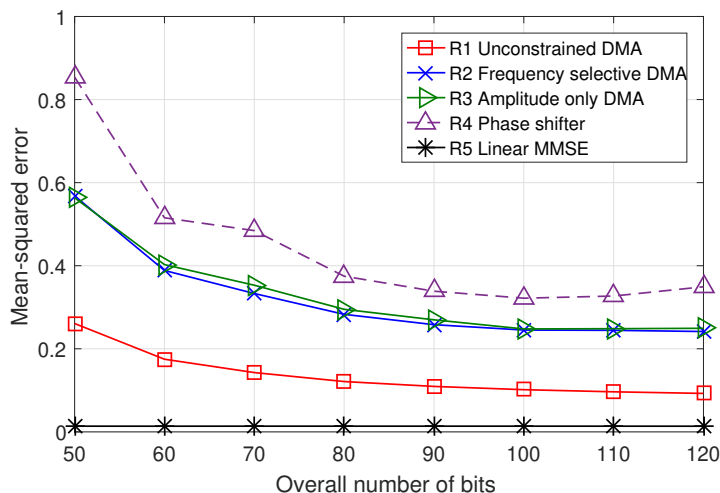


Fig. 8. MSE versus bits, SNR of 8 dB.

respect to the overall bit budget, compared to phase shifter based hybrid receivers as well as the unquantized linear MMSE estimator. To that aim, we depict in Figs. 8-9 the resulting signal recovery MSE and uncoded BER, respectively, of the considered receivers versus the bit budget $b_{\text{overall}} \in \{50, 120\}$ for an SNR of 8 dB. The BER achieved by the linear MMSE estimator operating without quantization constraints is significantly lower than that achieved by the bit-constrained receiver, and is thus not included in Fig. 9. Note that a fully-digital receiver, i.e., one in which each antenna element feeds a dedicated ADC as commonly assumed in MIMO communications receivers [30]–[32], [44], cannot be applied with less than $2N = 200$ bits. Consequently, all the considered values of b_{overall} correspond to BSs operating under strict bit

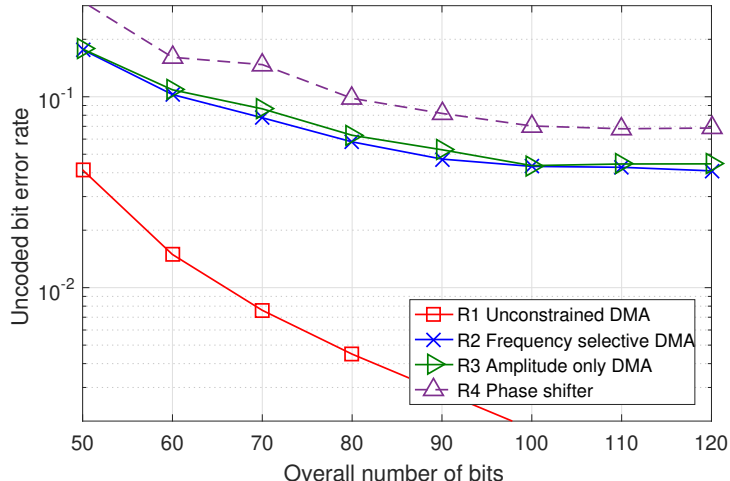


Fig. 9. Unencoded BER versus bits, SNR of 8 dB.

constraints. Observing Figs. 8-9, we note that the MSE and BER gains of the proposed designs, observed in Figs. 6-7 for receivers operating utilizing 80 bits for representing their channel output, hold for all considered values of b_{overall} .

To summarize, DMAs, which typically use less power and cost less than standard antenna arrays, can be utilized to implement a configurable frequency selective hybrid architecture. The results presented in this section demonstrate that by using our proposed methods, one can design a high-performance DMA-based receiver which is particularly suitable for bit-constrained MU-MIMO-OFDM setups, achieving notable performance gains over conventional phase shifter based receivers designed using previously proposed methods.

V. CONCLUSIONS

In this work we studied the application of DMAs, which realize low cost and power efficient configurable antenna arrays, for bit-constrained MU-MIMO-OFDM systems. We formulated a model for the received quantized DMA outputs which accounts for the adaptable frequency selective profile of the metamaterial elements, and showed that the OFDM recovery problem can be expressed as a task-based quantization setup. Next, we derived an iterative algorithm for setting the DMA weights, ignoring their structure constraints, to minimize the MSE in recovering the transmitted signal, by sequentially adapting each microstrip. Then, we proposed methods for approximating the unconstrained DMA using configurations which capture the physical properties of metasurfaces, considering both narrowband approximations of their operation as well as the more general Lorentzain-type wideband model. Our numerical results demonstrate the gains

of utilizing task-based quantization to determine the pre-quantization combining carried out in the DMA along with the ADC support and the digital processing. In particular, it is shown that by properly exploiting the physical characteristics of DMAs, OFDM symbol detection is significantly facilitated when operating under strict bit constraints.

APPENDIX

A. Proof of Proposition 1

It follows directly from the definition of \mathbf{Q} that $\mathbf{Q}^H \mathbf{Q} = \text{blkdiag}(\bar{\mathbf{q}}_1 \bar{\mathbf{q}}_1^H, \bar{\mathbf{q}}_2 \bar{\mathbf{q}}_2^H, \dots, \bar{\mathbf{q}}_{N_d} \bar{\mathbf{q}}_{N_d}^H)$. We define the following matrices to facilitate subsequent proof:

$$\mathbf{E}_j = \left[\underbrace{\mathbf{O}_{N_e} \cdots \mathbf{O}_{N_e}}_{j-1} \quad \mathbf{I}_{N_e} \quad \underbrace{\mathbf{O}_{N_e} \cdots \mathbf{O}_{N_e}}_{N_d-j} \right]^T,$$

$$\Phi_j = \left[\underbrace{\mathbf{O}_{N_e} \cdots \mathbf{O}_{N_e}}_{j-1} \quad (\bar{\mathbf{q}}_j \bar{\mathbf{q}}_j^H)^T \quad \underbrace{\mathbf{O}_{N_e} \cdots \mathbf{O}_{N_e}}_{N_d-j} \right]^T.$$

Clearly, $\Phi_j = \mathbf{E}_j \bar{\mathbf{q}}_j \bar{\mathbf{q}}_j^H \mathbf{E}_j^H$. Then the matrix $\mathbf{Q}^H \mathbf{Q}$ can be derived as

$$\mathbf{Q}^H \mathbf{Q} = \sum_{j=1}^{N_d} \Phi_j = \sum_{j=1}^{N_d} \mathbf{E}_j \bar{\mathbf{q}}_j \bar{\mathbf{q}}_j^H \mathbf{E}_j^H. \quad (\text{A.1})$$

Substituting (A.1) into (12) along with the block-diagonal expressions for $\bar{\mathbf{G}}$ and Σ , and the fact that the inverse of a block-diagonal matrix is block-diagonal with the inverse submatrices [41, Ch. 3.7], yields (13), proving the proposition. \square

REFERENCES

- [1] T. L. Marzetta, "Noncooperative cellular wireless with unlimited numbers of base station antennas," *IEEE Trans. Wireless Commun.*, vol. 9, no. 11, pp. 3590–3600, Nov. 2010.
- [2] M. Jiang and L. Hanzo, "Multiuser MIMO-OFDM for next-generation wireless systems," *Proc. IEEE*, vol. 95, no. 7, pp. 1430–1469, 2007.
- [3] Y. C. Eldar, *Sampling theory: Beyond bandlimited systems*. Cambridge University Press, 2015.
- [4] R. H. Walden, "Analog-to-digital converter survey and analysis," *IEEE J. Sel. Areas Commun.*, vol. 17, no. 4, pp. 539–550, 1999.
- [5] J. G. Andrews, S. Buzzi, W. Choi, S. V. Hanly, A. Lozano, A. C. Soong, and J. C. Zhang, "What will 5G be?" *IEEE J. Sel. Areas Commun.*, vol. 32, no. 6, pp. 1065–1082, 2014.
- [6] N. Shlezinger, Y. C. Eldar, and M. R. Rodrigues, "Hardware-limited task-based quantization," *IEEE Trans. Signal Process.*, vol. 67, no. 20, pp. 5223–5238, 2019.
- [7] S. Salamatian, N. Shlezinger, Y. C. Eldar, and M. Médard, "Task-based quantization for recovering quadratic functions using principal inertia components," in *Proc. IEEE ISIT*, 2019.

- [8] N. Shlezinger and Y. C. Eldar, "Deep task-based quantization," *arXiv preprint arXiv:1908.06845*, 2019.
- [9] X. Zhang, A. F. Molisch, and S.-Y. Kung, "Variable-phase-shift-based RF-baseband codesign for MIMO antenna selection," *IEEE Trans. Signal Process.*, vol. 53, no. 11, p. 4091, 2005.
- [10] R. Méndez-Rial, C. Rusu, N. González-Prelcic, A. Alkhateeb, and R. W. Heath, "Hybrid MIMO architectures for millimeter wave communications: Phase shifters or switches?" *IEEE Access*, vol. 4, pp. 247–267, 2016.
- [11] S. S. Ioushua and Y. C. Eldar, "A family of hybrid analog–digital beamforming methods for massive MIMO systems," *IEEE Trans. Signal Process.*, vol. 67, no. 12, pp. 3243–3257, 2019.
- [12] F. Sotrobiani and W. Yu, "Hybrid analog and digital beamforming for mmwave OFDM large-scale antenna arrays," *IEEE J. Sel. Areas Commun.*, vol. 35, no. 7, pp. 1432–1443, 2017.
- [13] N. Shlezinger, Y. C. Eldar, and M. R. Rodrigues, "Asymptotic task-based quantization with application to massive MIMO," *IEEE Trans. Signal Process.*, vol. 67, no. 15, pp. 3995–4012, 2019.
- [14] T. Gong, N. Shlezinger, S. S. Ioushua, M. Namer, Z. Yang, and Y. C. Eldar, "RF chain reduction for MIMO systems: A hardware prototype," *arXiv preprint arXiv:1905.05315*, 2019.
- [15] D. R. Smith, O. Yurduseven, L. Pulido-Mancera, P. Bowen, and N. B. Kundtz, "Analysis of a waveguide-fed metasurface antenna," *Phys. Rev. Applied*, vol. 8, no. 5, Nov. 2017.
- [16] D. R. Smith, V. R. Gowda, O. Yurduseven, S. Larouche, G. Lipworth, Y. Urzhumov, and M. S. Reynolds, "An analysis of beamed wireless power transfer in the fresnel zone using a dynamic, metasurface aperture," *Journal of Applied Physics*, vol. 121, no. 1, p. 014901, 2017.
- [17] T. Slesman, M. F. Imani, W. Xu, J. Hunt, T. Driscoll, M. S. Reynolds, and D. R. Smith, "Waveguide-fed tunable metamaterial element for dynamic apertures," *IEEE Antennas Wireless Propag. Lett.*, vol. 15, pp. 606–609, 2016.
- [18] A. V. Diebold, M. F. Imani, T. Slesman, and D. R. Smith, "Phaseless computational ghost imaging at microwave frequencies using a dynamic metasurface aperture," *Appl Opt.*, vol. 57, no. 9, pp. 2142–2149, 2018.
- [19] C. Huang, A. Zappone, G. C. Alexandropoulos, M. Debbah, and C. Yuen, "Reconfigurable intelligent surfaces for energy efficiency in wireless communication," *IEEE Trans. Wireless Commun.*, vol. 18, no. 8, pp. 4157–4170, 2019.
- [20] M. Di Renzo, M. Debbah, D.-T. Phan-Huy, A. Zappone, M.-S. Alouini, C. Yuen, V. Sciancalepore, G. C. Alexandropoulos, J. Hoydis, H. Gacanin *et al.*, "Smart radio environments empowered by reconfigurable AI meta-surfaces: an idea whose time has come," *EURASIP Journal on Wireless Communications and Networking*, vol. 2019, no. 1, pp. 1–20, 2019.
- [21] P. del Hougne, M. Fink, and G. Lerosey, "Optimally diverse communication channels in disordered environments with tuned randomness," *Nature Electronics*, vol. 2, no. 1, p. 36, 2019.
- [22] W. Tang, X. Li, J. Y. Dai, S. Jin, Y. Zeng, Q. Cheng, and T. J. Cui, "Wireless communications with programmable metasurface: Transceiver design and experimental results," *China Communications*, vol. 16, no. 5, pp. 46–61, 2019.
- [23] J. Y. Dai, W. K. Tang, J. Zhao, X. Li, Q. Cheng, J. C. Ke, M. Z. Chen, S. Jin, and T. J. Cui, "Wireless communications through a simplified architecture based on time-domain digital coding metasurface," *Advanced Materials Technologies*, vol. 4, no. 7, p. 1900044, 2019.
- [24] N. Shlezinger, O. Dicker, Y. C. Eldar, I. Yoo, M. F. Imani, and D. R. Smith, "Dynamic metasurface antennas for uplink massive MIMO systems," *IEEE Trans. Commun.*, vol. 67, no. 10, pp. 6829–6843, 2019.
- [25] H. Wang, N. Shlezinger, S. Jin, Y. C. Eldar, I. Yoo, M. F. Imani, and D. R. Smith, "Dynamic metasurface antennas based downlink massive MIMO systems," in *Proc. IEEE SPAWC*, 2019, pp. 1–5.
- [26] I. Yoo, M. F. Imani, T. Slesman, H. D. Pfister, and D. R. Smith, "Enhancing capacity of spatial multiplexing systems using reconfigurable cavity-backed metasurface antennas in clustered MIMO channels," *IEEE Trans. Commun.*, vol. 67, no. 2, pp. 1070–1084, Feb. 2018.

- [27] M. C. Johnson, S. L. Brunton, N. B. Kundtz, and J. N. Kutz, "Sidelobe canceling for reconfigurable holographic metamaterial antennas," *IEEE Trans. Antennas Propag.*, vol. 63, no. 4, pp. 1881–1886, Apr. 2015.
- [28] I. F. Akyildiz and J. M. Jornet, "Realizing ultra-massive MIMO (1024×1024) communication in the (0.06–10) terahertz band," *Nano Communication Networks*, vol. 8, pp. 46–54, 2016.
- [29] K. Roth, H. Pirzadeh, A. L. Swindlehurst, and J. A. Nossek, "A comparison of hybrid beamforming and digital beamforming with low-resolution ADCs for multiple users and imperfect CSI," *IEEE J. Sel. Topics Signal Process.*, vol. 12, no. 3, pp. 484–498, June 2018.
- [30] J. Mo, P. Schniter, and R. W. Heath, "Channel estimation in broadband millimeter wave MIMO systems with few-bit ADCs," *IEEE Trans. Signal Process.*, vol. 66, no. 5, pp. 1141–1154, 2017.
- [31] S. Jacobsson, G. Durisi, M. Coldrey, U. Gustavsson, and C. Studer, "Throughput analysis of massive MIMO uplink with low-resolution ADCs," *IEEE Trans. Wireless Commun.*, vol. 16, no. 6, pp. 4038–4051, 2017.
- [32] J. Choi, J. Mo, and R. W. Heath, "Near maximum-likelihood detector and channel estimator for uplink multiuser massive MIMO systems with one-bit ADCs," *IEEE Trans. Commun.*, vol. 64, no. 5, pp. 2005–2018, 2016.
- [33] D. R. Smith, J. B. Pendry, and M. C. K. Wiltshire, "Metamaterials and negative refractive index," *Science*, vol. 305, no. 5685, p. 788792, Aug. 2004.
- [34] C. L. Holloway, E. F. Kuester, J. A. Gordon, J. O'Hara, J. Booth, and D. R. Smith, "An overview of the theory and applications of metasurfaces: The two-dimensional equivalents of metamaterials," *IEEE Antennas Propag. Mag.*, vol. 54, no. 2, pp. 10–35, Apr. 2012.
- [35] J. Hunt, T. Driscoll, A. Mrozack, G. Lipworth, M. Reynolds, D. Brady, and D. R. Smith, "Metamaterial apertures for computational imaging," *Science*, vol. 339, no. 6117, pp. 310–313, 2013.
- [36] T. M. Cover and J. A. Thomas, *Elements of information theory*. John Wiley & Sons, 2012.
- [37] R. W. Heath and G. B. Giannakis, "Exploiting input cyclostationarity for blind channel identification in OFDM systems," *IEEE Trans. Signal Process.*, vol. 47, no. 3, pp. 848–856, 1999.
- [38] S. Wei, D. L. Goeckel, and P. A. Kelly, "Convergence of the complex envelope of bandlimited OFDM signals," *IEEE Trans. Inf. Theory*, vol. 56, no. 10, pp. 4893–4904, 2010.
- [39] J. Hoydis, S. Ten Brink, and M. Debbah, "Massive mimo in the ul/dl of cellular networks: How many antennas do we need?" *IEEE J. Sel. Areas Commun.*, vol. 31, no. 2, pp. 160–171, 2013.
- [40] N. Shlezinger and Y. C. Eldar, "On the spectral efficiency of noncooperative uplink massive MIMO systems," *IEEE Trans. Commun.*, vol. 67, no. 3, pp. 1956–1971, 2019.
- [41] C. D. Meyer, *Matrix analysis and applied linear algebra*. Siam, 2000.
- [42] B. Ghogh, F. Karray, and M. Crowley, "Eigenvalue and generalized eigenvalue problems: Tutorial," *arXiv preprint arXiv:1903.11240*, 2019.
- [43] D. W. Marquardt, "An algorithm for least-squares estimation of nonlinear parameters," *Journal of the society for Industrial and Applied Mathematics*, vol. 11, no. 2, pp. 431–441, 1963.
- [44] H. Wang, W. Shih, C. Wen, and S. Jin, "Reliable OFDM receiver with ultra-low resolution ADC," *IEEE Trans. Commun.*, vol. 67, no. 5, pp. 3566–3579, May 2019.
- [45] C. Xiao, J. Wu, S.-Y. Leong, Y. R. Zheng, and K. B. Letaief, "A discrete-time model for triply selective MIMO rayleigh fading channels," *IEEE Trans. Wireless Commun.*, vol. 3, no. 5, pp. 1678–1688, 2004.
- [46] W. C. Jakes and D. C. Cox, *Microwave mobile communications*. Wiley-IEEE Press, 1994.
- [47] D. M. Pozar, *Microwave engineering*. John Wiley & Sons, 2009.